

Influence of Target Cavity Formation on the Emission Spectra of Nanosecond Laser Ablation Plasmas^{*)}

James Edward A. HERNANDEZ II, Shinnosuke YAMADA, Shouta SASAKI,
Allen Vincent CATAPANG and Motoi WADA

Graduate School of Science and Engineering, Doshisha University, Kyotanabe, Kyoto 610-0394, Japan

(Received 10 January 2022 / Accepted 20 February 2022)

Optical emission spectroscopy as well as time-of-flight (TOF) measurements were performed in the diagnostics of nanosecond laser produced plasmas. The target is rotated during pulsed laser ablation at 5 GW/cm^2 , where the optical emission spectroscopy is performed along, as well as perpendicular to the target axis. Parallel to the target axis, the continuum radiation intensity increases up to 6000 pulses, and emission line intensities from C I and C II increase for with number of pulses. Perpendicular to the target axis, decrease in emission line and continuum intensities were observed. TOF measurements resulted to carbon cluster ions detection from C_n^+ , $n \geq 2$, where peak shift of $4 \mu\text{s}$ towards later times were observed after 10000 pulses ablation. Charge collection experiments showed approximately 80 percent energy loss after 10000 shots. Collision-induced recombination mechanisms were suggested as causes of energy loss and line intensity decrease.

© 2022 The Japan Society of Plasma Science and Nuclear Fusion Research

Keywords: laser induced breakdown spectroscopy, laser ablation, optical emission spectroscopy

DOI: 10.1585/pfr.17.2406018

1. Introduction

Laser induced breakdown spectroscopy (LIBS) is the process involving the optical diagnostics of radiating plasma produced by a high powered laser above the target vaporization threshold [1]. LIBS has garnered significant attention due to its ease in sample preparation, as the spectral information about the sample can be obtained by a single laser shot [2]. LIBS has been employed in space applications, such as the analysis of Martian soils, where carbon is one of the main elements of study [3]. Carbon plasmas produced by laser ablation have also been explored in the production of clusters, including fullerene-like films [4]. In laser produced carbon plasmas, the conditions for cluster formation highly depend on the background environment under which the plasma is initiated [5,6].

When the focused laser ablates the target, a small crater is embedded on the target as the plasma undergoes free expansion. Repeatedly ablating the same spot should vary the plasma characteristics, as a hole is formed on the target. Initiating the plasma deep in the cavity would confine the plasma expansion, thus signifying the contribution of the target in the variation of the plasma characteristics. In LIBS, the optical spectrum of the laser-produced plasma is observed from the surface, that is, under the condition of plasma plume free expansion. Assuming a high density on the target surface, kinetic models such as the unsteady adiabatic expansion describe the plasma propagation [7]. However, in the condition where a hole is formed by the

laser, and the plasma is initiated deep within this target cavity formed by repeatedly ablating the same spot, the spectral characteristics of the plasma at this region has not yet been extensively investigated. For a laser produced plasma in a cavity, not only that the plasma constituents, but the inner cavity walls also influence the plasma expansion. In this work, a laser ablation device is developed to directly compare the emission spectra of a carbon plasma observed from the target surface with the region directed along the target axis. Diagnostic methods involved in characterizing the laser plasma are optical emission spectroscopy (OES) and time-of-flight spectrometry (TOF).

2. Experimental Details

Figure 1 (a) shows the experimental setup for the collection of emission spectra. A nanosecond Q-switched Nd:YAG laser (pulse width = 5 ns, $\lambda = 1064 \text{ nm}$) is incident 12 degrees from the axis of a cylindrical graphite pellet target using a converging lens ($f = 300 \text{ mm}$). The target diameter and height are 10 mm, and 20.5 mm, respectively. The laser creates a spot diameter around 1 mm at the center of the target surface. The laser is aligned so that the ablation spot is the same during rotation at 20 revolutions per minute via a DC motor attached to a vacuum rotational motion feedthrough. The emission spectra are collected from two sides: parallel and perpendicular to the target axis via viewport flange attachments. For both arrangements, a converging lens ($f = 150 \text{ mm}$) focuses light towards an optical fiber connected to an emission spectrometer (USB4000). The data rate of the CCD array of the

author's e-mail: cyjd3302@mail4.doshisha.ac.jp

^{*)} This article is based on the presentation at the 30th International Toki Conference on Plasma and Fusion Research (ITC30).

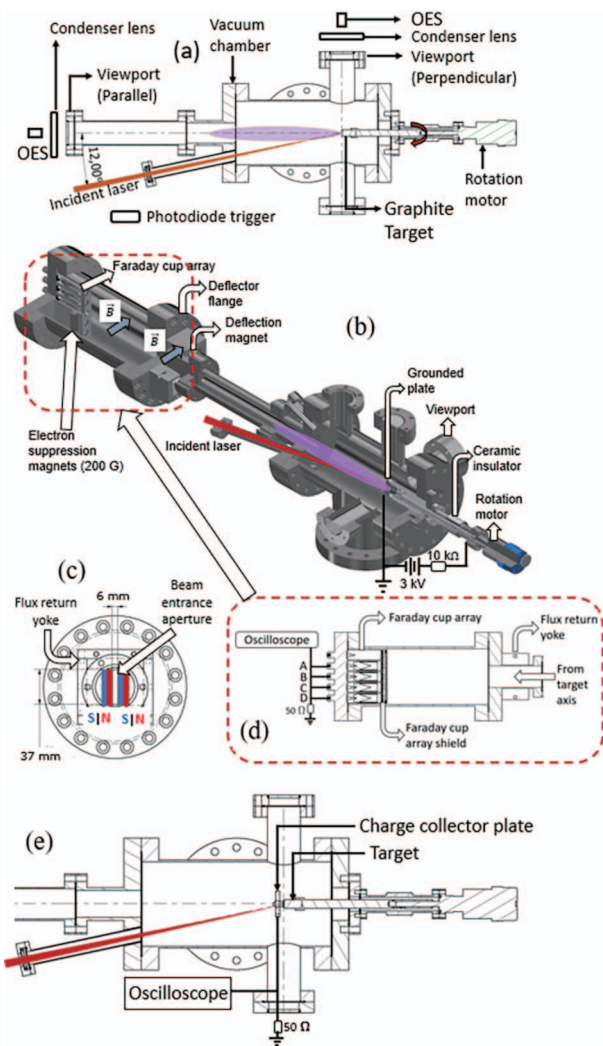


Fig. 1 (a) Laser ablation schematic for emission spectra collection (b) TOF measurement schematic (c) Faraday cup array schematic (d) Deflection region schematic (e) Near-target charge collection experiment schematic.

spectrometer is approximately 0.5 MHz. The wavelength, and sensitivity of the as-received spectrometer were calibrated. However, effects due to the degradation of the internal components of the spectrometer were not evaluated. Nevertheless, the purpose of this work is to compare the relative intensity of the emission spectra parallel and perpendicular to the target axis, thereby foregoing the need for identifying the absolute emission intensity for each corresponding wavelength. The integration time of the spectrometer is set to 1 s to ensure collection of the spectra. An average of 10 spectra is collected during laser ablation at 10 Hz repetition rate. Spectra are collected for every 1000 pulses up to 10000 pulses at 5 GW/cm² laser intensity. The time evolution of the emission spectra in LIBS is typically recorded. However, since the aim of this work is to compare the accumulated emission spectra in both parallel and perpendicular regions of the constricted discharge, and estimating an apparent temperature from these spectra,

the time-resolved emission measurement is not performed. Moreover, obtaining the time-resolved spectra with delay times below 1 μs, typically performed in LIBS is beyond the capability of the optical emission spectrometer employed in this work.

In order to investigate the ions present in the laser plasma, the target is biased at 3 kV extraction voltage via a stainless steel target holder while a 5 mm thick aluminum grounded plate is placed 5 mm from the target surface. Then, a time-of-flight (TOF) spectrometer is assembled, as shown in Fig. 1 (b), where the incident port of the spectrometer replaces the viewport attachment parallel to the target axis. Neodymium magnets were installed 47 cm from the target which deflect the incoming laser produced plasma at a 200 G magnetic field intensity. Figure 1 (c) shows the schematic of the deflection flange. The flange consists of a 37 mm by 6 mm aperture for the incident beam. Neodymium permanent magnets with peak flux density of 670 G are installed, where the deflection magnetic field induces a Lorentz force in the direction of the gravitational force. The total deflection region distance is 4 cm. The TOF signals are collected at an average of 16 pulses at 5 GW/cm² laser intensity. The TOF spectrometer consists of a Faraday cup array with four terminals situated approximately 65 cm from the target, shown in Fig. 1 (d). Each of the cups is terminated by a 50 Ω resistor, and are labelled A-D, where the distance between the axes of each cup is 18 mm. Faraday cup A collects the current against the Lorentz force direction. Faraday cup B collects the current directed along the target axis. Faraday cups C and D collect signals which are deflected along the Lorentz force direction. Electron suppression magnets with 300 G flux density are attached to the grounded Faraday cup array shield.

Figure 1 (e) shows the schematic for the near-target collection experiment, where current signals from the expanding plume are collected by a 5 mm thick aluminum plate with a 9 mm aperture. The plate is placed 5 mm from the target surface, and is connected to an oscilloscope terminated by a 50 Ω resistor. Experiments are performed at 6 × 10⁻⁶ Pa pressure.

3. Results

3.1 Emission spectra of the laser plasma parallel and perpendicular to the target axis

Figure 2 shows the emission spectra collected parallel and perpendicular to the target axis. In both directions, the spectra consist of a superposition of multiple carbon peaks ranging from C I to C IV, and continuum radiation. For the emission spectra parallel to the target axis shown in Fig. 2 (a), the continuum radiation is present up to approximately 930 nm, with the peak at 500 nm. On the other hand, the continuum radiation is present up to 800 nm for the case of 0 to 1000 pulses ablation perpendicular to the

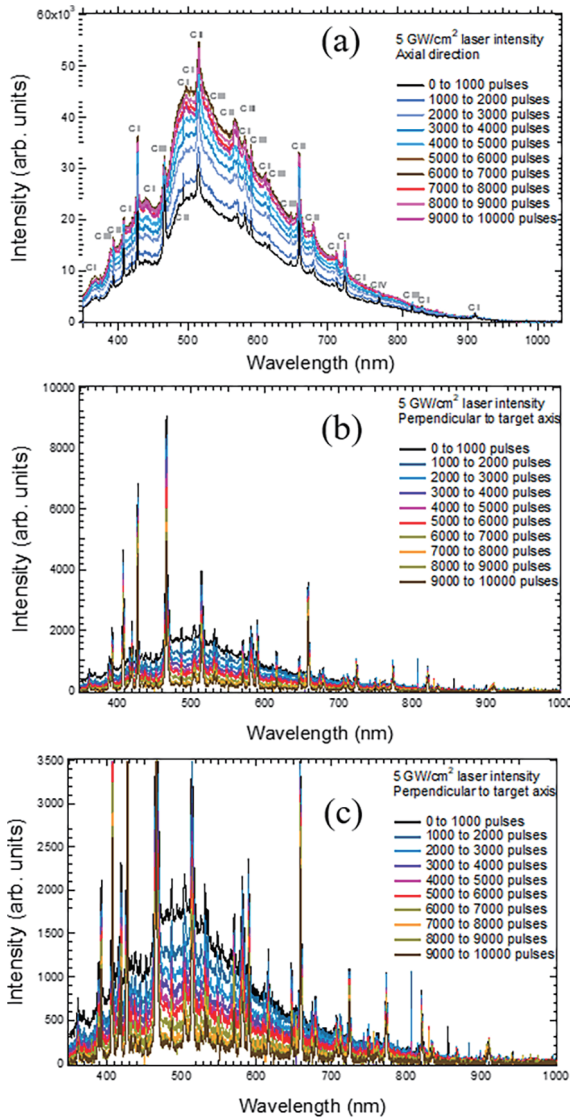


Fig. 2 Emission spectra of carbon laser ablation plasma directed (a) parallel and (b) perpendicular to the target axis (c) Emission spectra perpendicular to the target axis expanded at the ordinate.

target axis shown in Figs. 2 (b) and (c), where the continuum peak ranges from 480 to 520 nm. The carbon species are identified assuming the peaks represent atomic transitions, whose spectroscopic data are obtained from NIST database [8].

Figure 3 shows the continuum radiation intensity evolution for increasing number of laser pulses. The intensities for both parallel and perpendicular directions are normalized with respect to that after 1000 pulses ablation. Increase in continuum intensities are observed parallel to the target axis until 6000 pulses, where the peak intensity at 510 nm reached almost twice that of the intensity after 1000 shots. Further increasing the number of pulses after 6000 shots results to a decrease in the continuum emission intensity. For the direction perpendicular to the target axis, the continuum emission intensity decreases to around 15

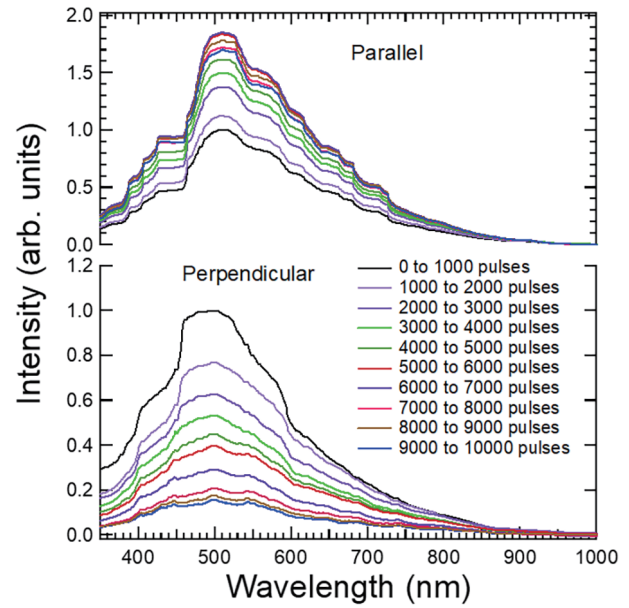


Fig. 3 Continuum intensity evolution increasing number of pulses.

percent of that of after 1000 pulses intensity. After which, the rate of intensity decrease slows down after 8000 pulses.

In the emission spectra involving laser induced breakdown of carbon, the continuum was treated as a Planck-like distribution [9, 10]. However, in this work, the case of thermal equilibrium is not assumed, thus it is noted also that the distribution is not strictly a conventional blackbody. The continuum intensity is fitted under such distribution in order to quantify the evolution of continuum radiation intensity in the formation of the cavity. In the frequency parametrization, the intensity $I_{pl}(\nu, T)$ is then given by

$$I_{pl}(\nu, T) = G\nu^5 e^{-h\nu/kT}, \quad (1)$$

where G, ν, h, k, T are the exponential prefactor, emission frequency, Planck constant, Boltzmann constant, and apparent continuum temperature, respectively. Taking the natural logarithm of both sides, we have

$$\ln\left(\frac{I_\nu}{\nu^5}\right) = \ln G - \frac{h\nu}{kT}, \quad (2)$$

where the apparent temperature can be obtained from the slope of the line formed by (I_ν/ν^5) versus ν . Figure 4 shows the apparent continuum temperature for increasing number of pulses. Since the left-hand side of Eq. 2 in the entire optical frequency range consists of a positive and negative slope, only the region with the negative slope, corresponding to wavelengths from 500 nm was taken. Within this region, the following optical frequency ranges were chosen: 500 - 358 nm, 500 - 374 nm, 500 - 390 nm, 500 - 405 nm, and 500 - 421 nm. The spectra corresponding to these optical frequencies were fitted to Eq. 2 where, from the slope, the average and the standard deviation of the apparent temperature are obtained. Fitting was performed on

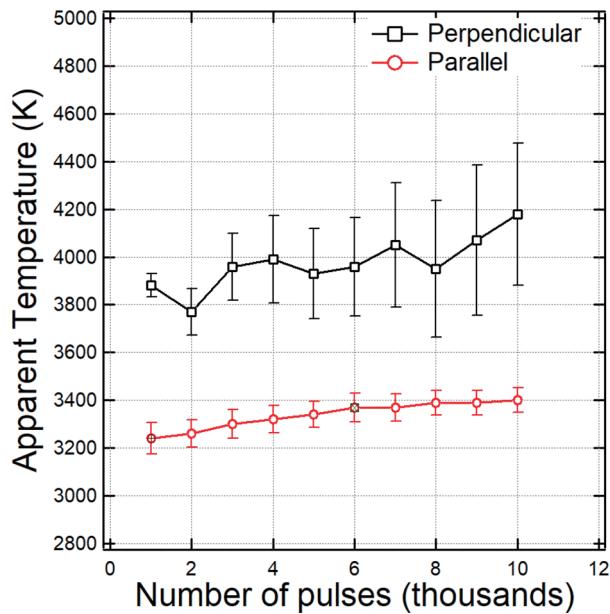


Fig. 4 Apparent continuum temperature for increasing number of pulses in the parallel and perpendicular directions.

the spectra from 1000 to 10000 pulses. The obtained apparent temperature is plotted with the number of pulses and is shown in Fig. 4. The estimated apparent continuum temperature is higher in the perpendicular direction than that in parallel direction. The obtained standard deviation of the apparent temperature in the parallel direction ranges from 51 to 65 K, while a deviation from 48 to 316 K is calculated in the perpendicular direction. An increase of approximately 200 K in the average apparent temperature in the perpendicular direction for increasing pulses is observed, whose rate decreased after 6000 shots. No significant correlation in the apparent temperature with the number of pulses is observed in the perpendicular direction.

Since the emission spectra consist of atomic transitions and continuum radiation, the latter should be subtracted in order to observe the evolution of the carbon emission line transitions as the number of pulses is increased. Performing this subtraction, the peak evolution of the emission line intensities corresponding to emission lines of C I (427.0 nm, $2s^22p3s \leftarrow 2s^22p5p$), C II (514.0 nm, $2s2p(^3P^o)3s \leftarrow 2s2p(^3P^o)3p$), C III (465.2 nm, $1s^22s3s \leftarrow 1s^22s3s$), and C IV (772.8 nm) are shown in Fig. 5. For the spectra directed perpendicular to the target axis, decrease of approximately 40 percent is observed for the C III ion after 10000 pulses ablation. The intensity change perpendicular to the target is plotted with an exponential fit, where C II has the highest rate of decrease with a calculated rate constant of 5.7×10^{-5} /pulse. A similar trend was observed for the C I, C III, and C IV lines in this direction. On the other hand, the emission line evolution for increasing number of pulses parallel to the target axis shows an initial increase in the C I intensity from after 1000 pulses to after 4000 pulses, and in C II intensity from

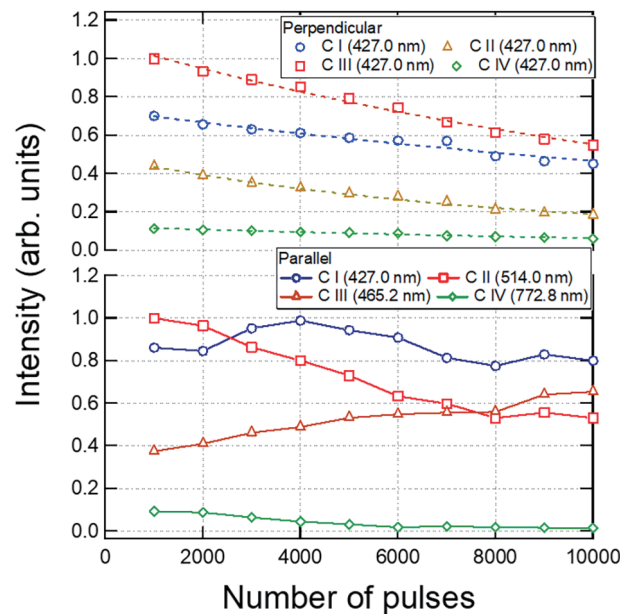


Fig. 5 Emission line peak evolution of carbon spectral lines from C I to C IV for increasing number of pulses, dashed lines represent exponential fits.

after 1000 pulses to 10000 pulses. The C III and C IV line emission intensities decrease as the number of pulses is increased, where the rate of decrease of C III slows down after 8000 pulses. The intensity of C III is higher than that of C I until after 2000 pulses, while the C II emission exceeds that of C III from after 8000 pulses. Parallel to the target axis, the emission intensity increases up to 7000 pulses, followed by a subsequent decrease for increasing number of pulses. On the other hand, the emission spectra perpendicular to the target axis decreases for increasing number of pulses.

3.2 Time-of-flight measurements

In order to identify the ionic species which propagate from the expanding plasma, TOF measurements are performed. Figure 6 shows the TOF spectra for the fresh and after 10000 pulses condition at 3 kV extraction voltage and 5 GW/cm^2 laser intensity. The highest peak current signal is collected from the Faraday cup labelled C, whose axis is located 18 mm from that of the target axis. A number of cluster ions ranging from C_2^+ detected at $4.1 \mu\text{s}$ to C_{50}^+ at $20.8 \mu\text{s}$ were identified. Increasing number of pulses decreases the overall signal intensity, reducing to approximately $6 \mu\text{A}$ peak amplitude. The positive signals also shift towards later times, where the C_2^+ peak shift is approximately $4 \mu\text{s}$. A negative signal is detected by Faraday cup A at approximately $5.2 \mu\text{s}$, which correspond to negative carbon ions. Figure 7 shows the current signals collected 5 mm from the target surface for the fresh target without the cavity, after 1000 pulses, and after 10000 pulses ablation. Initial negative peaks at 9, 16, and 22 ns correspond

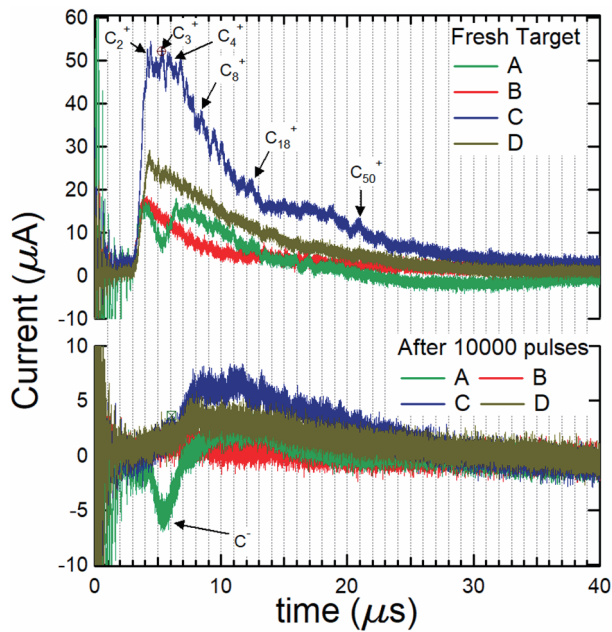


Fig. 6 Faraday cup array signals for (a) fresh target and (b) after 10000 pulses ablation.

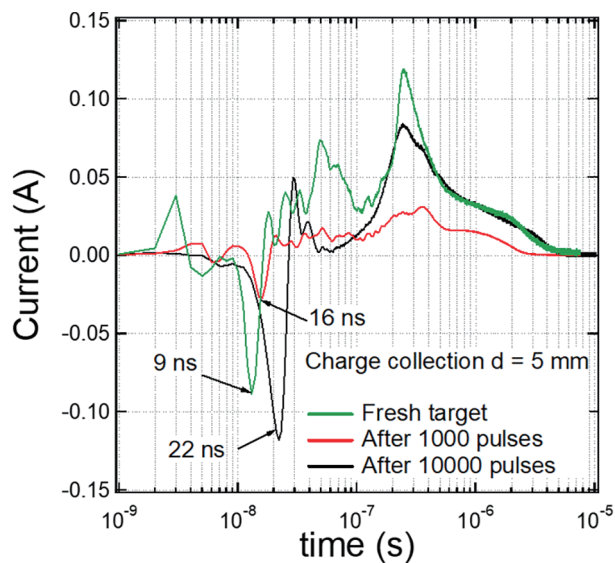


Fig. 7 Current signals collected 5 mm from the target for increasing number of pulses at 5 GW/cm^2 laser intensity.

to electrons for the fresh target, after 1000 pulses, and after 10000 pulses ablation respectively. The negative peaks are then followed by positive ion signals starting from 30 ns, which persist until 30 μs .

4. Discussion

The laser plasma emission spectra consist of both emission lines and continuum radiation. For the former, the detection of higher ionization levels corresponding to C III and C IV shown in Fig. 2 is due to the space charge during the formation of the laser plasma. At the onset of



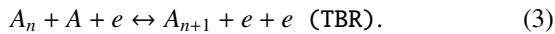
Fig. 8 Graphite target cross section after 10000 pulses.

plasma formation, electrons are first ejected from the target surface which induces an electric field with the target [11]. The electrons are then followed by heavier ions, as also shown in the current signals in Fig. 7. Some electrons follow the trajectory of the plasma expansion direction with energy gained from the incident laser, while others follow the direction of the positively charged target opposite to the expansion direction. The latter electrons contribute to the further ionization of the excited species via electron impact. The ionization probability also contributes to the line intensity, which explains the low intensity of C IV ion. After 10000 pulses at 5 GW/cm^2 , the target cavity is formed with a diameter of 0.7 mm and cavity depth of 2 mm, as shown in Fig. 8. The decrease of higher energy states correspond to the increased electron-ion recombination within the cavity. This leads to the increase in lower charge state intensity shown in Fig. 5, where the decrease and increase of C III and C II line intensities are observed, respectively. The increase and subsequent decrease of the emission line intensity of C I suggests the excitation and de-excitation processes occurring within the cavity, respectively, as the plume is confined to a small volume. As the hole depth increases, the recombination probability increases, leading to the collision-induced de-excitation of higher energy states. In the perpendicular direction, however, all line spectra exhibit a decaying behavior as the number of pulses is increased, showing the decreasing number of ions able to escape with the increase of cavity depth.

The emission spectra also exhibit broad energy distributions leading to wide continuum radiation bands which range from the target ionization threshold to higher energies [12]. Parallel to the target axis, the increase in continuum intensity until 6000 pulses shown in Fig. 3 suggests the constriction of plasma expansion, leading to an increased probability of collision-induced radiative recombination. An increase of approximately 200 K in the average apparent temperature in this direction after 6000 pulses also supports the hypothesis of increased radiative recombination within the cavity. Beyond which, the rate slows down suggesting the decrease in ablation rate as the number of pulses is increased [13]. Moreover, the expansion of ions, electrons, and neutrals ejected by the laser is hindered by the cavity, leading to collision-induced energy losses. These losses are shown from the shift in the TOF peak towards later times after 10000 pulses, as shown in the Faraday cup D in Fig. 6. The continuum emission in-

tensity corresponding to C II at 514 nm is highest in the direction parallel to the target axis, which shows a high amount of recombining ions in this wavelength range. Perpendicular to the target axis, only the radiation bands originating from the electrons and ions which have recombined outside the cavity are detected, which explains the lower continuum radiation intensity in this region, and its further reduction as the number of pulses is increased. Therefore, most of the recombining processes occur within the cavity leading to a high continuum radiation intensity, while mechanisms leading to ionic transitions dominate as these ions have high enough energy to escape the hole. Moreover, the higher apparent temperature in the perpendicular direction relative to the parallel direction suggests that the electrons outside the surface recombine at a higher energy. The error increase of the apparent temperature in the perpendicular direction as the number of pulses is increased is reflected on the low continuum intensity.

The TOF signals show the ions which propagate after the plasma plume expansion. As shown in Fig. 6, the laser plasma also consisted of cluster ions, whose intensities decrease as the number of pulses is increased. The highest signal intensity at Faraday cup C shows the deflected ions 18.5 mm from the target axis. A possible mechanism for the ion intensity decrease for increasing number of pulses is the three-body recombination (TBR) caused by the cavity, given by



As the hole is formed on the target, the laser plasma expansion is hindered by the cavity walls which serve as collision regions for the laser produced plume. At 10000 pulses, the peak shift towards later times indicates ion energy losses as inelastic collisions occur inside the plume before propagating towards the detectors. For an ion with mass m , flight path d and energies ϵ_1 and ϵ_2 corresponding to times-of-flight t_1 and t_2 for the fresh and after 10000 pulse ablation respectively, the energy loss can be estimated by

$$\epsilon_2 - \epsilon_1 = \frac{1}{2}md^2 \left(\frac{1}{t_2^2} - \frac{1}{t_1^2} \right). \quad (4)$$

For a C_2^+ ion with $d = 650$ mm, $t_1 = 4$ μ s, $t_2 = 8$ μ s, the energy loss corresponds to 2.4 keV, or 100 eV per nucleon. After 10000 pulses, the existence of a negative signal at Faraday cup A (directed opposite to the deflection field) indicates that negative ions also formed suggesting electron attachment, which is also caused by collisions induced by the cavity walls [13]. These negative ions are formed upstream from the deflection region, which capture electrons and are deflected opposite to the Lorentz force direction once they pass through the aperture with the bending magnet. From the charge collection results, the electron kinetic energy can be estimated for a fresh target, that is, without a cavity, to be 0.87 eV. From Eq. 4, the energy loss corre-

sponds to 0.73 eV, after 10000 pulses ablation. This indicates the energy losses exhibited by the electrons as they underwent inelastic collisions with the target cavity. The trend of the TOF current signal decrease for increasing number of pulses is similar to the emission line intensity decrease observed in the region perpendicular to the target. Since the species detected outside the cavity involve the propagating ions in the expanding plume, the ion species detected in the TOF measurements after 10000 pulses are those with energy capable of escaping the target cavity. During the initiation phase of the laser plasma, ejection of electrons is followed by that of positively charged ions and neutral atoms. At the time at which the ions are accelerated, the space charge in front of the target is positive. As these ions propagate downstream before the deflection region, electrons and neutrals undergo collisions which produces electrons. These electrons attach to neutrals thus forming negative ions. The mass of these negative ions is suggested to be that of C^- rather than that of higher mass carbon, since fragmentation, along with collisional electron detachment occurs on higher mass carbon clusters [14]. These negative signals are shown to be ions rather than electrons due to the path integral flux density of approximately 1.8 kG cm integrated along the deflection region distance of 4 cm. The TOF measurements in Fig. 6 showed the peak shift towards later times as the number of pulses is increased. This indicates that mechanisms leading to cluster formation are also observed. Energy losses in the cavity lead to increase in collision-induced cooling, which facilitate the cluster formation via condensation mechanism. However, the competing processes of ion fragmentation also occurs, as more ions are collisionally excited and de-excited in the cavity, as observed in the increase in continuum line intensity and temperature in Figs. 3 and 4. Further increase in laser shots above 8000 pulses in all optical emission spectra measurements lead to the slower rate of decrease in both line and continuum intensity due to the decrease in ablation depth, leading to lower amount of recombining ions.

5. Conclusions

Diagnostics of laser plasmas produced by nanosecond ablation of a rotating graphite target are performed by OES and TOF, for which a system for characterizing the solid sample at its surface, and at the region in which a cavity is formed is developed. OES measurements for the axial and perpendicular direction are taken during pulsed laser ablation in order to investigate the mechanisms occurring at the surface, as well as inside the cavity. Emission spectra directed parallel to the target axis exhibited higher continuum radiation intensity than that perpendicular to the axis, indicating collision-induced excitation occurs within the target hole leading to broad frequency bands. Emission spectral line intensities are shown to be higher perpendicular to the target axis, which decrease as the number of

pulses increase. TOF measurements also show the detection of carbon clusters C_n^+ , $n \geq 2$, where the ion signals decrease after 10000 pulses ablation. The role of the cavity is the increase in collision probability leading to ion energy losses. Charge collection experiments also showed the energy losses exhibited the electrons in the presence of the cavity. The increase of cavity formation constricts the expanding plasma, and enhances the radiative recombination at the broad frequency as observed in the continuum radiation intensity increase. The cavity also contributes to ion fragmentation and current and line intensity decrease as measured from the TOF and OES, respectively. The origin of the continuum spectra emission enhancement by the cavity, and its correlation with the detected species from the TOF will be further investigated. Moreover, the time-resolved measurements on the optical spectra will provide information on the evolution of the expanding plasma from the cavity.

- [1] J.P. Singh and S. Thakur, ed., *Laser-Induced Breakdown Spectroscopy* (Elsevier, Cambridge, 2007) p. 3-5.
- [2] R. Gaudioso, M. Dell'Aglio, O. De Pascale, G.S. Senesi and A. De Giacomo, *J. Sens.* **10**, 7434 (2010).
- [3] L. Radziemski, D.A. Cremers, K. Benelli, C. Khoo and R.D. Harris, *Spectrochim. Acta B* **60**, 237 (2005).
- [4] A.A. Voevodin, J.G. Jones and J.S. Zabinski, *J. Appl. Phys.* **92**, 724 (2002).
- [5] T. Kerdja, S. Abdelli, D. Ghobrini and S. Malek, *J. Appl. Phys.* **80**, 5360 (1996).
- [6] A.A.I. Khalil, *Laser Phys.* **20**, 238 (2010).
- [7] M. Capitelli, A. Casavola, G. Colonna and A. De Giacomo, *Spectrochim. Acta B* **59**, 271 (2004).
- [8] National Institute of Standards and Technology (NIST) Atomic Spectra Database, NIST Atomic Spectra Database (U.S. Department of Commerce, 1999), http://physics.nist.gov/cgi-bin/AtData/main_asd
- [9] L. Nemes, A.M. Keszler, C.G. Parigger, J.O. Hornkohl, H.A. Michelsen and V. Stakhursky, *Appl. Opt.* **46**, 19 (2007).
- [10] A. De Giacomo, R. Gaudioso, M. Dell'Aglio and A. Santagata, *Spectrochim. Acta B* **65**, 385 (2010).
- [11] T. Mościcki, J. Hoffman and Z. Szymański, *Arch. Mech.* **63**, 2, 99 (2011).
- [12] T. Fujimoto, *Plasma Spectroscopy* (Clarendon Press, Oxford, 2004) p. 205-212.
- [13] J.E. Hernandez and M. Wada, *AIP Conf. Proc.* **2373**, 090004 (2021).
- [14] R. Rajeev, T. Madhu Trivikram, K.P.M. Rishad, V. Narayanan and M. Krishnamurthy, *New J. Phys.* **15**, 043036 (2013).